The Astrophysical Journal, 652:1020–1027, 2006 December 1
© 2006. The American Astronomical Society. All rights reserved. Printed in U.S.A.

# AN EXACT, THREE-DIMENSIONAL, TIME-DEPENDENT WAVE SOLUTION IN LOCAL KEPLERIAN FLOW

Steven A. Balbus
École Normale Supérieure, Laboratoire de Radioastronomie, 24 Rue Lhomond, 75231 Paris Cedex 05, France

and

John F. Hawley
Astronomy Department, University of Virginia, Charlottesville, VA 22903
*Received 2006 June 2; accepted 2006 August 5*

## ABSTRACT

We present an exact three-dimensional wave solution to the shearing-sheet equations of motion. The existence of this solution argues against transient amplification as a route to turbulence in unmagnetized disks. Moreover, because the solution covers an extensive dynamical range in wavenumber space, it is an excellent test of the dissipative properties of numerical codes.

*Subject headings:* accretion, accretion disks — galaxies: magnetic fields — instabilities — magnetic fields — MHD

## 1. INTRODUCTION

The combination of magnetic fields and differential rotation is a volatile one, leading to the magnetorotational instability (MRI) under very general conditions (e.g., Balbus 2003). Laboratory evidence for the MRI in liquid sodium has recently been claimed (Sisan et al. 2004), and there can be little doubt that in magnetized disks the MRI will be present and a source of the enhanced angular momentum transport needed for accretion to proceed. But not all astrophysical disks need be everywhere ionized at a level at which the field and the gas are well coupled. Therefore, the question of whether or not an unmagnetized, laminar gas in Keplerian rotation is vulnerable to turbulent breakdown continues to attract attention.

The nature of the local stability of Keplerian disks has been investigated by detailed numerical simulation (Balbus et al. 1996; Hawley et al. 1999). There is no evidence of nonlinear instability. Indeed, the notion that Keplerian disks are intrinsically turbulent would be most surprising and problematic to MHD numericists, who routinely check the validity of an MHD code by ensuring that the disk quickly returns to stability when the magnetic field is removed. Even when nonlinear perturbations are directly seeded, they do not lead to turbulence.

Numerical simulations have been criticized, however, on the grounds that they lack the necessary resolution to reveal nonlinear instabilities (e.g., Richard & Zahn 1999; Afshordi et al. 2005). The claim is that the effective Reynolds number of available codes is too low, and that the numerical schemes dissipate nascent nonlinear instabilities. In some cases, a specific destabilizing mechanism is suggested. Afshordi et al. (2005) suggest, for example, that the transient growth exhibited by linear nonaxisymmetric perturbations, in the course of evolving from leading to trailing wavenumbers, might become sufficiently large to cross a threshold and initiate nonlinear turbulence.

The first systematic numerical studies of Keplerian stability are now a decade old, and numerical codes have developed and improved. Our physical understanding of disks has also deepened. We are motivated to reexamine the problem of the stability of Keplerian disks. In this paper we present precise analytic solutions for three-dimensional incompressible perturbations in Keplerian disks, recovering the previously known two-dimensional solutions as special cases. We show that in fact all such solutions are valid both linearly and nonlinearly, because the nonlinear terms in the equations of motion vanish. Thus, these solutions by themselves do not trigger nonlinear instabilities, regardless of the level of transient amplification attained. Since the solutions exhibit both strongly leading and strongly trailing large wavenumbers, they cover a very large dynamical range. They are, in fact, a good test of the dissipation properties of numerical codes. Conversely, the numerical codes test the stability of these exact time-dependent solutions, which would otherwise be a difficult analytic calculation.

Recently, laboratory experiments have weighed in on the controversy. A high Reynolds number ($\sim 10^6$) Couette flow experiment found that Keplerian-like profiles are nonlinearly stable (H. Ji 2006, private communication). This finding is compatible with numerical simulations, but in conflict with an earlier experiment (Richard 2001) that claimed that such profiles were unstable. The Ji experiment uses differentially rotating end caps to break up Ekman boundaries (which otherwise cause unwanted interior circulation), and Doppler velocimetry techniques to verify that the rotation profiles matched their analytic counterparts. The Reynolds stress in the Ji experiment has also been measured, and residual fluctuations in the radial and azimuthal velocities are uncorrelated; the tensor vanishes on average.

These results are compelling reasons to believe that local Keplerian flow is nonlinearly stable, and that the numerical simulations have not been prohibitively dissipative or otherwise qualitatively misrepresentative. The explicit solutions we present in this paper will provide numericists with a well-posed numerical test bed that will sharpen our understanding of local small-scale behavior in Keplerian disks.

An outline of this paper is as follows. In § 2 we provide an overview of the issues that have been debated. Section 3 sets up the mathematical background, and the full analysis is given in § 4. The solutions derived in § 4 are applied as a code test problem in § 5. Finally, § 6 summarizes our work.

## 2. A BRIEF REVIEW

Axisymmetric waves propagating in the interior of an unmagnetized disk are stable if and only if the specific angular momentum $l$ increases with cylindrical radius $R$. This is the classical Rayleigh-stability criterion, and it is generally satisfied in astrophysical disks. When stable, fluid displacements in the disk plane

oscillate about their equilibrium circular orbits with a characteristic frequency $\kappa$. The value of $\kappa^2$ is directly proportional to the specific angular momentum gradient $l$. In particular,

$$\kappa^2 = \frac{1}{R^3}\frac{dl^2}{dR} = 4\Omega^2 + \frac{d\Omega^2}{d\ln R}, \quad (1)$$

where $R$ is the cylindrical radius and $\Omega = l/R^2$ is the local disk angular velocity. The formal transition to a negative value of $\kappa^2$ corresponds to the onset of rotational instability. It is to be noted that this result applies only to axisymmetric disturbances; there is at present no known rigorous nonaxisymmetric criterion (hence, the ongoing debate). A radially discontinuous rotation profile, for example, would be unstable to nonaxisymmetric disturbances by the Kelvin-Helmholtz instability, even if the rotation rate increased outward and was formally Rayleigh-stable.

For a Keplerian disk, $\kappa^2 = \Omega^2$, which is a stable profile by the Rayleigh criterion. In the absence of pressure forces, this is unconditionally stable; the behavior of Keplerian orbits is not an object of current debate. Pressure forces must therefore be at the heart of any proposed instability mechanism. This is already a potential difficulty for proponents of instability, since any system that is close to Keplerian must be characterized by very small radial background pressure gradients, and perturbative pressure gradients generally behave acoustically. Even global instabilities in flows that would be locally Rayleigh-stable revert to stable behavior as the disk approaches a Keplerian profile (see, e.g., Goldreich et al. 1986).

The claims to nonlinear instability discussed in § 1 are of course meant to apply to systems that are linearly stable. It is not unprecedented for linear waves to be subject to a finite amplitude instability (e.g., Infeld & Rowlands 1990), and even at arbitrarily small amplitudes, one-dimensional adiabatic sound waves show nonlinear steepening behavior. (In fact, the shearing-wave solutions to be discussed are, in their tightly wrapped phase, subject to dissipative instabilities that may well prevent them from achieving even modest amplitudes.) But proponents of nonlinear Keplerian instability are arguing for something far more novel than wave modification. The claim is that well-behaved local linear disturbances that formally begin and end their existence as small amplitude waves, heavily dominated by restoring forces, in actuality become self-sustaining turbulence. If only the small nonlinear terms were properly resolved, it is argued, the simulations would reveal this behavior. In this view, current disk codes would be not merely imprecise, but grossly misrepresentative of the most fundamental character of Keplerian flow.

Planar Couette and Poiseuille viscous flows are two classic shear profiles that exhibit a breakdown into turbulence. Their behavior has motivated the notion that Keplerian rotation ought to do the same. Planar Couette flow is linearly stable (in a marginal sense) but nonlinearly unstable, whereas Poiseuille flow is linearly unstable if the appropriately defined Reynolds number Re exceeds a large critical value ($\mathrm{Re}_{\mathrm{crit}} = 5772$; see, e.g., Drazin & Reid 1981 for details). Both flows are exquisitely sensitive to nonlinear disturbances.

Planar Poiseuille and Couette flows have boundary layers and linear dynamical responses lacking a dominant restoring force. The presence of viscous boundary layers means that the Reynolds number is an important feature of the flow stability, and at the same time allows for linear instability in Poiseuille flow at a sufficiently high Reynolds number. By way of contrast, local Keplerian flow has no viscous boundary layers, and its destabilizing shear is strongly stabilized by the Coriolis force, $2\Omega > |d\Omega/d\ln R|$. It is not surprising, therefore, that the response of disks is sensitive to neither the Reynolds number, nor the amplitude of the initial disturbances.

The mechanism by which shear flow nonlinearly breaks down into turbulence seems to be fairly well understood, at least in its essentials; nonlinear perturbations are in essence linear disturbances that feed off of a marginally stable, finite-amplitude two-dimensional perturbation that is imposed on the shear flow (Zahn et al. 1974; Bayly et al. 1988). If no such marginally stable, finite-amplitude state exists—and for Keplerian disks it does not—the mechanism breaks down. In fact, detailed numerical simulations show no tendency for Keplerian rotation to evolve toward self-sustained turbulence, even when driven vigorously well into the nonlinear regime by a sympathetic programmer. A revealing example is the case of thermally driven convective turbulence. In the Boussinesq limit, this results in a very small but measurable angular momentum flux with the wrong sign to sustain turbulence (Stone & Balbus 1996).[1] Moreover, even codes with very different small-scale dissipation properties converge when presented with the same initial set of finite-amplitude disturbances (Hawley et al. 1999). Such convergence would hardly be expected if each code were anomalously dissipative in its own way.

The current work is supportive of numerical simulation and the recent Ji laboratory experiment. The analytic perturbation solutions are in fact *exact* solutions to the dynamical equations. The nonlinear terms that are supposed to trigger turbulence instead vanish. This is problematic for the idea that these disturbances seed turbulence. More positively, it is an opportunity to test the accuracy of current codes. The solutions can be determined to any desired order of accuracy either by well-established Wentzel-Kramers-Brillouin (WKB) techniques or by direct numerical integration of a simple ordinary differential equation (ODE). The waveforms involve time-dependent wavenumbers of arbitrarily high magnitudes, both leading and trailing. Despite the fact that the amplitude of the departure from Keplerian flow can be made arbitrarily high, the solution remains formally valid. Secondary instabilities feeding off this finite-amplitude wave cannot be excluded a priori, but in fact the recent findings of Shen et al. (2006) suggest that such secondary instabilities make matters even more difficult. Very tightly wound leading-wave solutions (which would evolve toward the largest amplitudes) break down in the early stages of their evolution by what seems to be a Kelvin-Helmholtz instability. Far from becoming nonlinear, the wave dissipates before there is any appreciable growth.

## 3. PRELIMINARIES

### 3.1. *The Shearing Box*

The "shearing box" is the mathematical limit of the equations of motion in cylindrical coordinates that corresponds to retaining the local behavior of differentially rotating flow. The approach has a long history, dating at least as far back as the classical two-dimensional "shearing-sheet" calculation of Goldreich & Lynden-Bell (1965). A more recent MHD description can be found in the review article of Balbus & Hawley (1998). The idea is that one looks at the flow very near a fixed cylindrical radius $R$ and takes the limit as $R \to \infty$. The angular velocity $\Omega$ remains finite, and the azimuthal velocity $v_\phi$ formally increases without bound. We

[1] A negative Reynolds stress, which cannot be due to numerical dissipation, poses difficulties for the notion that Keplerian disks are formally turbulent, but at a level too small to be detected (Lesur & Longaretti 2005). Shear turbulence, whatever its magnitude, can be sustained only by a *positive* Reynolds stress.

are interested in departures from the Keplerian profile $v_\phi = v_K$, defined by

$$\boldsymbol{u} = \boldsymbol{v} - v_K \boldsymbol{e}_\phi, \tag{2}$$

where $\boldsymbol{v}$ is the exact velocity and $\boldsymbol{e}_\phi$ is a unit vector in the azimuthal direction. Note that the $\boldsymbol{u}$-velocities are taken relative to the radially changing Keplerian profile, not relative to a frame that is rotating at a constant angular velocity. The unperturbed flow is thus $\boldsymbol{u} = 0$, and $|\boldsymbol{u}|$ is always small compared with the large quantity $v_\phi$.

In a standard $R, \phi, z$ cylindrical coordinate system, the inviscid equations of motion in the local shearing-box limit are ( Balbus & Hawley 1998)

$$\frac{Du_R}{Dt} - 2\Omega u_\phi = -\frac{1}{\rho}\frac{\partial P}{\partial R}, \tag{3}$$

$$\frac{Du_\phi}{Dt} + \frac{\kappa^2}{2\Omega} u_R = -\frac{1}{\rho R}\frac{\partial P}{\partial \phi}, \tag{4}$$

$$\frac{Du_z}{Dt} = -\frac{1}{\rho}\frac{\partial P}{\partial z} - z\Omega^2, \tag{5}$$

where

$$\frac{D}{Dt} = \frac{\partial}{\partial t} + \Omega\frac{\partial}{\partial \phi} + \boldsymbol{u}\cdot\nabla. \tag{6}$$

Our notation is as follows: $\rho$ is the mass density of the disk, $P$ is the gas pressure, and $\kappa^2$ is the epicyclic frequency associated with departures from circular orbits (eq. [1]). Formally, the local vertical gravitational force is $-z\Omega^2$ for a Keplerian potential. However, it is often ignored in shearing-box calculations (the "cylindrical approximation"), and we generally do so in this paper.

As noted, the equations apply to a local radial neighborhood around a large radius, $R$. The coefficients $2\Omega$, $\kappa^2/2\Omega$, and $\Omega^2$ are regarded as local constants. Finally, the equation for mass conservation in our constant-density system is simply

$$\nabla\cdot\boldsymbol{u} = 0. \tag{7}$$

It is to be emphasized that these equations, while local, are fully nonlinear.

It is also informative to write the shearing-box equations in a frame that is rotating at a fixed angular velocity. Fix $R$ to be the radius at the center of the box, and fix $\Omega = \Omega(R)$. Let $x$ be the radial distance from $R$, $y = R(\phi - \Omega t)$, and $z$ the vertical distance from the midplane. With

$$\boldsymbol{w} = \boldsymbol{v} - R\Omega\boldsymbol{e}_\phi, \tag{8}$$

in their most general form the shearing-box dynamical equations are

$$\left(\frac{\partial}{\partial t} + \boldsymbol{w}\cdot\nabla\right) w_R - 2\Omega w_\phi = -x\frac{d\Omega^2}{d\ln R} - \frac{1}{\rho}\frac{\partial P}{\partial x}, \tag{9}$$

$$\left(\frac{\partial}{\partial t} + \boldsymbol{w}\cdot\nabla\right) w_\phi + 2\Omega w_R = -\frac{1}{\rho}\frac{\partial P}{\partial y}, \tag{10}$$

$$\left(\frac{\partial}{\partial t} + \boldsymbol{w}\cdot\nabla\right) w_z = -z\Omega^2 - \frac{1}{\rho}\frac{\partial P}{\partial z}. \tag{11}$$

(We have retained the vertical force in eq. [11].) Mass conservation is

$$\frac{\partial \rho}{\partial t} + \nabla\cdot(\rho\boldsymbol{w}) = 0. \tag{12}$$

In this form, equations (9)–(12) are sometimes referred to as the Hill equations.

The Hill equations have a simple scaling symmetry:

$$\boldsymbol{w}(\boldsymbol{r}, t) \leftrightarrow \epsilon\boldsymbol{w}(\boldsymbol{r}/\epsilon, t), \tag{13}$$

$$\rho(\boldsymbol{r}, t) \leftrightarrow \rho(\boldsymbol{r}/\epsilon, t), \tag{14}$$

$$P(\boldsymbol{r}, t) \leftrightarrow \epsilon^2 P(\boldsymbol{r}/\epsilon, t). \tag{15}$$

In this form, with $\epsilon \ll 1$ we see that any solution of the Hill equations that involves very small length scales has a rescaled magnified counterpart with exactly the same time dependence. Any instability at small scales would also have to be unstable at larger scales.

### 3.2. *Shearing Coordinates*

We next introduce the coordinate transformation (Goldreich & Lynden-Bell 1965)

$$\phi' = \phi - \Omega t = \phi - t[\Omega(R) + x\, d\Omega/dR], \tag{16}$$

in which we have expanded $\Omega$ in a Taylor series about radius $R$ ($x$ is a small excursion from a fiducial value of $R$). The other coordinate transformations are identities, $t' = t$, $R' = R$, and $z' = z$. The transformed partial derivatives are

$$\frac{\partial}{\partial t} + \Omega\frac{\partial}{\partial \phi} = \frac{\partial}{\partial t'}, \tag{17}$$

$$\frac{\partial}{\partial R} = \frac{\partial}{\partial R'} - t\frac{d\Omega}{dR}\frac{\partial}{\partial \phi'}, \tag{18}$$

$$\frac{\partial}{\partial z} = \frac{\partial}{\partial z'}, \qquad \frac{\partial}{\partial \phi} = \frac{\partial}{\partial \phi'}. \tag{19}$$

The explicit form of the equations of motion is

$$\frac{\partial u_R}{\partial t'} + \boldsymbol{u}\cdot\nabla u_R - 2\Omega u_\phi = -\frac{1}{\rho}\left(\frac{\partial}{\partial R'} - t'\frac{d\Omega}{dR}\frac{\partial}{\partial \phi'}\right)P, \tag{20}$$

$$\frac{\partial u_\phi}{\partial t'} + \boldsymbol{u}\cdot\nabla u_\phi + \frac{\kappa^2}{2\Omega}u_R = -\frac{1}{\rho R}\frac{\partial P}{\partial \phi'}, \tag{21}$$

$$\frac{\partial u_z}{\partial t'} + \boldsymbol{u}\cdot\nabla u_z = -\frac{1}{\rho}\frac{\partial P}{\partial z'}, \tag{22}$$

where

$$\boldsymbol{u}\cdot\nabla = u_R\left(\frac{\partial}{\partial R'} - t'\frac{d\Omega}{dR}\frac{\partial}{\partial \phi'}\right) + \frac{u_\phi}{R}\frac{\partial}{\partial \phi'} + u_z\frac{\partial}{\partial z'}. \tag{23}$$

Mass conservation is

$$\left(\frac{\partial}{\partial R'} - t'\frac{d\Omega}{dR}\frac{\partial}{\partial \phi'}\right)u_R + \frac{1}{R}\frac{\partial u_\phi}{\partial \phi'} + \frac{\partial u_z}{\partial z'} = 0. \tag{24}$$

These equations form the basis of the analysis of § 4.

## 4. ANALYSIS

### 4.1. *Reduction to a Single ODE*

The system of equations (20)–(24) has no spatial dependence but does depend explicitly on time $t'$. This suggests that we seek a solution of the form

$$f(t')\exp\left[i\left(k_R'R' + m\phi'/R' + k_z z'\right)\right], \tag{25}$$

where the function $f$ will of course differ for each of the velocity components and the pressure. Without loss of generality, we can take $m > 0$. Note that because of vanishing velocity divergence, the nonlinear $(\boldsymbol{u}\cdot\nabla)\boldsymbol{u}$ terms vanish explicitly. Indeed, the $\boldsymbol{u}\cdot\nabla$ operator acting on any perturbed modal plane wave vanishes. One can immediately see why nonlinear rotational hydrodynamic instabilities are problematic: linear theory and nonlinear theory are the same for a finite-amplitude plane wave.

Although a superposition of these shearing waves would not be a solution of the nonlinear equations, in order to sustain turbulence such a superposition would have to somehow access the free energy source of differential rotation. But in general, the neglected nonlinear $(\boldsymbol{u}\cdot\nabla)\boldsymbol{u}$ wave term leads not to a viable free energy source but to mutual wave-wave interactions. Without a steady source term directly linked to the differential rotation, it is perhaps not surprising that these wave-wave cascades do not seem to be self-sustaining.

In what follows, the fluid velocity $\boldsymbol{u}$ and pressure $P$ variables refer to the time-dependent Fourier $f$ amplitude of equation (25). We define the unprimed time-dependent wavenumber

$$k_R \equiv k_R(t') = k_R' - t' m\frac{d\Omega}{dR}, \tag{26}$$

and henceforth drop the prime superscript from $t'$ and other coordinates that are identical in both frames, and write $d/dt$ for the time derivative of the amplitudes. The equations of motion are

$$\frac{du_R}{dt} - 2\Omega u_\phi = -ik_R\frac{P}{\rho}, \tag{27}$$

$$\frac{du_\phi}{dt} + \frac{\kappa^2}{2\Omega}u_R = -i\frac{m}{R}\frac{P}{\rho}, \tag{28}$$

$$\frac{du_z}{dt} = -ik_z\frac{P}{\rho}, \tag{29}$$

and the equation of mass conservation is

$$u_R k_R + m u_\phi/R + k_z u_z = 0. \tag{30}$$

An equation for $u_R$ can be extracted from equations (26)–(30) after some straightforward, but tedious, algebra:

$$\frac{d^2u_R}{dt^2} - \frac{4k_R m}{k^2 R}\frac{d\Omega}{d\ln R}\frac{du_R}{dt} + \left[\frac{k_z^2}{k^2}\kappa^2 + \frac{2m^2}{k^2R^2}\left(\frac{d\Omega}{d\ln R}\right)^2\right]u_R = 0, \tag{31}$$

where

$$k^2 \equiv k_R^2(t) + \frac{m^2}{R^2} + k_z^2. \tag{32}$$

This equation is in fact mathematically equivalent to equation (56) of Johnson & Gammie (2005a). These authors have shown that it can be solved in terms of hypergeometric functions. Here we prefer to take a somewhat different tack, which avoids the introduction of rather complicated special functions. A pleasant simplification ensues if we introduce the variable

$$U = k^2 u_R. \tag{33}$$

Then our differential equation takes on the compact Schrödinger form:

$$\frac{d^2U}{dt^2} + \frac{k_z^2}{k^2}\kappa^2 U = 0, \tag{34}$$

and is amenable to a classical WKB analysis.

#### 4.1.1. *Explicit Solutions*

Equation (34) can be written in a convenient dimensionless form. Let

$$k_\perp^2 = k_z^2 + (m/R)^2, \quad k_\perp > 0, \tag{35}$$

and introduce a new time variable $\tau$:

$$\tau \equiv \frac{k_R(t)}{k_\perp}. \tag{36}$$

Since $d\Omega/dR < 0$ for the problems of interest,

$$\frac{d\tau}{dt} = -\frac{m}{k_\perp}\frac{d\Omega}{dR} > 0. \tag{37}$$

With this substitution, our differential equation becomes

$$\frac{d^2U}{d\tau^2} + \frac{\beta^2}{1+\tau^2}U = 0, \tag{38}$$

with

$$\beta = \left|\frac{k_z\kappa/m}{d\Omega/dR}\right|. \tag{39}$$

The leading-order WKB solution of this equation is

$$U \sim \left(1+\tau^2\right)^{1/4}\exp\left(\pm i\beta\sinh^{-1}\tau\right), \tag{40}$$

or

$$u_R = u_R(0)\left(1+\tau^2\right)^{-3/4}\exp\left(\pm i\beta\sinh^{-1}\tau\right), \tag{41}$$

where $u_R(0)$ is defined to be $u_R$ at $t = 0$. Formally, this breaks down in the limit $\tau \gg \beta$, but in practice very little changes. The differential equation for $U$ can be easily solved to leading order in the overlapping asymptotic domain $\tau \gg 1$. For $\beta \geq \frac{1}{4}$

$$u_R = \text{const}\times\tau^{-3/2}\exp\left[\pm i\beta(1-1/4\beta^2)^{1/2}\ln\tau\right], \tag{42}$$

while for $\beta \leq \frac{1}{4}$

$$u_R = \text{const}\times\tau^{-\left(3\pm\sqrt{1-4\beta^2}\right)/2}. \tag{43}$$

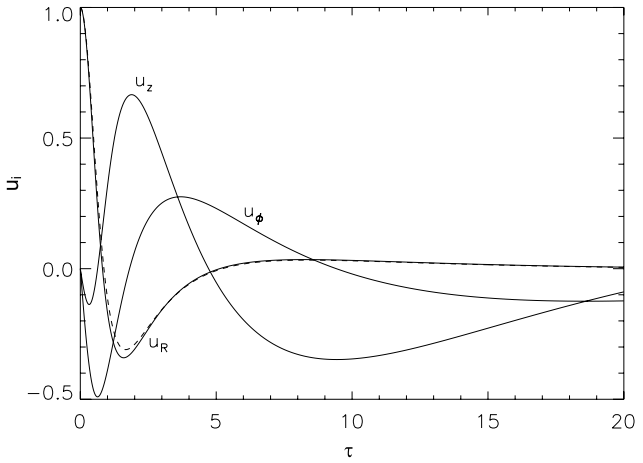



FIG. 1.—Radial ($u_R$), azimuthal ($u_\phi$), and axial ($u_z$) velocity components for disturbances in a $\beta = 2$ Keplerian disk. For reference, the radial velocity WKB solution (*dashed line*) lies almost directly on top of the exact solution $u_R$, appearing slightly above the true solution near the minimum point.

With the precise leading-order large-$\tau$ solution in hand we see that equation (41) is actually valid in the domain $\ln\tau \ll 8\beta$. For $\beta = 2$, for example, this corresponds to $\tau \ll 10^7$, considerably larger than the naive domain of applicability, $\tau \lesssim \beta = 2$. Even beyond the extended domain, however, the WKB solution differs from the actual large-$\tau$ solution only by a slowly varying phase. We henceforth adopt equation (41) as our formal solution for $u_R$.

#### 4.1.2. *Solution for the Pressure and Nonradial Velocities*

To complete the problem, we require expressions for $u_\phi$, $u_z$, and $P$. Unlike $u_R$, these flow variables need not have a simple WKB form. Nevertheless, they can be obtained explicitly in terms of $u_R(\tau)$ and $du_R/d\tau$.

The key is to note that equation (38) can be written

$$u_R = -\frac{1}{\beta^2}\frac{d^2}{d\tau^2}\left[\left(1+\tau^2\right)u_R\right], \tag{44}$$

which implies

$$\int u_R(\tau)\,d\tau = -\frac{1}{\beta^2}\frac{d}{d\tau}\left[\left(1+\tau^2\right)u_R\right] + \text{const.} \tag{45}$$

If we combine equations (28), (29), and (30),

$$\frac{k_\perp^2}{k_z^2}\frac{du_\phi}{dt} + \frac{\kappa^2}{2\Omega}u_R + \frac{m}{Rk_z^2}\frac{d(k_R u_R)}{dt} = 0. \tag{46}$$

Writing this in terms of $\tau$ and simplifying,

$$\frac{d}{d\tau}\left(u_\phi + \frac{m\tau u_R}{k_\perp R}\right) + \frac{m\beta^2}{2k_\perp R}\left|\frac{d\ln\Omega}{d\ln R}\right|u_R = 0. \tag{47}$$

Finally, we integrate over $\tau$ and use equation (45). We find

$$u_\phi + \frac{m\tau u_R}{k_\perp R}\left(1 - \left|\frac{d\ln\Omega}{d\ln R}\right|\right) - \frac{m}{2k_\perp R} \times \left|\frac{d\ln\Omega}{d\ln R}\right|\left(1+\tau^2\right)\frac{du_R}{d\tau} = 0, \tag{48}$$

where the integration constant on the right has been set to zero to be consistent with the equation of motion (27). This determines $u_\phi$ in terms of $u_R$ and its first derivative,

$$u_\phi = \frac{m}{k_\perp R}\left[u_R\tau\left(\left|\frac{d\ln\Omega}{d\ln R}\right| - 1\right) + \frac{1+\tau^2}{2}\left|\frac{d\ln\Omega}{d\ln R}\right|\frac{du_R}{d\tau}\right]. \tag{49}$$

Next, the axial velocity $u_z$ is obtained from $\nabla\cdot\boldsymbol{u} = 0$,

$$u_z = -\frac{k_z}{k_\perp}\left[\tau u_R\left(1 + \frac{m^2}{R^2k_z^2}\left|\frac{d\ln\Omega}{d\ln R}\right|\right) + \frac{m^2}{2R^2k_z^2}\left|\frac{d\ln\Omega}{d\ln R}\right|\left(1+\tau^2\right)\frac{du_R}{d\tau}\right]. \tag{50}$$

The enthalpy $P/\rho$ then follows from equation (27):

$$\frac{P}{\rho} = -\frac{2\Omega i}{k_\perp}\left[u_R\left(\left|\frac{d\ln\Omega}{d\ln R}\right| - 1\right) + \frac{m\tau}{2k_\perp R}\left|\frac{d\ln\Omega}{d\ln R}\right|\frac{du_R}{d\tau}\right], \tag{51}$$

where it is understood that the real part of the equation is to be taken. This is convenient if $u_R$ is given as a WKB wave of the form of equation (41), which is precisely how we use it. Choosing

$$u_R = \mathrm{Re}\left[\frac{u_R(0)\exp\left(i\beta\sinh^{-1}\tau\right)}{\left(1+\tau^2\right)^{3/4}}\right] = \frac{u_R(0)\cos\left(\beta\sinh^{-1}\tau\right)}{\left(1+\tau^2\right)^{3/4}}, \tag{52}$$

we define the argument

$$X \equiv \beta\sinh^{-1}\tau, \tag{53}$$

and for Keplerian flow one obtains

$$u_\phi = -u_R(0)\left[\frac{k_z}{k_\perp}\frac{\sin X}{2(1+\tau^2)^{1/4}} + \frac{m}{k_\perp R}\frac{5\tau\cos X}{8(1+\tau^2)^{3/4}}\right], \tag{54}$$

$$u_z = u_R(0)\left[\frac{m}{2k_\perp R}\frac{\sin X}{(1+\tau^2)^{1/4}} - \frac{k_z}{k_\perp}\frac{\tau\cos X}{(1+\tau^2)^{3/4}}\left(1 + \frac{3m^2}{8k_\perp^2R^2}\right)\right], \tag{55}$$

$$\frac{P}{\rho} = \frac{u_R(0)\Omega}{k_\perp}\left[\frac{k_z}{k_\perp}\frac{\cos X}{(1+\tau^2)^{5/4}} + \frac{1+\tau^2(1-9m/4k_\perp R)}{(1+\tau^2)^{7/4}}\sin X\right]. \tag{56}$$

The velocity profiles are shown in Figure 1.

### 4.2. *The Small-$\beta$ Limit*

The presence of the $\beta$-term is a strongly stabilizing influence (it embodies epicyclic motion), and one therefore should examine the conditions under which it vanishes. In a Keplerian disk, $\kappa = \Omega$, and thus $\beta \ll 1$ must imply $k_zR \ll m$, which can correspond to one of two different physical situations. The first is when $u_z$ is a constant and all other variables vanish. These strictly vertical displacements are of little interest. The second possibility

corresponds to degenerate incompressible two-dimensional disturbances in the disk plane. This problem has been considered by other authors (Chagelishvili et al. 2003; Johnson & Gammie 2005a). When $\beta \to 0$, we drop the second term in equation (38) and find the formal result

$$u_R \sim \frac{C_1 + C_2\tau}{1+\tau^2}, \tag{57}$$

where $C_1$ and $C_2$ are constants of integration. This is consistent, of course, with equation (43) for large $\tau$. But in this limit, equations (27), (28), and (30) can be directly combined into the first-order equation

$$\frac{dU}{d\tau} = \frac{d(k^2 u_R)}{d\tau} = 0, \tag{58}$$

so that $C_2$ must be zero. (It represents a spurious solution.) Chagelishvili et al. suggest that the growing phase of these solutions ($\tau < 0$) may lead to turbulence, but we have seen that this solution is in fact exact. It cannot, and in simulations does not, lead to sustainable turbulence.

All of this stands in stark contrast to the case of a vanishing specific angular momentum gradient ($\kappa^2 = 0$), which does in fact lead to turbulence. Despite the apparently similar mathematics, the physical behavior of this $\beta = 0$ solution is very different. Why?

It is because in the case of $\kappa^2 = 0$, finite $\boldsymbol{k} = k_z \boldsymbol{e}_z$ *axisymmetric* modes now are algebraically unstable. Without the steady march toward arbitrarily large radial wavenumbers that cuts off nonaxisymmetric perturbations, axisymmetric $u_R$ perturbations continue to grow linearly with time. This solution is no longer a spurious branch of equation (34); it is a valid solution of the $m = \kappa = 0$ limit of equations (27)–(30). (Note that $\beta$ is actually undefined in this singular limit, and $\tau$ becomes a constant; one must work directly with $t$.) Perturbations in $u_\phi$ remain constant if $m = 0$, and grow linearly with time if the disturbance is even the slightest bit nonaxisymmetric. For a single mode, these are still exact nonlinear solutions, but an ensemble of modes in this case does lead to a turbulent cascade. The difference here is that the cascade can be fed by the axisymmetric instability, which features a consistently positive value for $-u_R u_\phi \, d\Omega/dR$, and thus a robust source of free energy. Indeed, in the axisymmetric limit, equations (27) and (29) combine to give

$$u_R u_\phi = \frac{1}{4\Omega}\frac{k^2}{k_z^2}\frac{du_R^2}{dt} > 0, \tag{59}$$

so that outward angular momentum transport accompanies the release of free energy, growing linearly with time in the early stages. By contrast, nonaxisymmetric solutions can maintain a source of free energy only for leading waves; this source becomes a sink when the waves become trailing. Unlike the uniform angular momentum turbulence, which is self-sustaining, fresh leading waves are always needed in Keplerian disks. Without them, perturbations die.

## 5. SIMULATIONS

Numerical simulations have sharpened our understanding of the stability of Keplerian disks. These calculations are not infallible, of course; they are subject to the limitations that accompany any solution by numerical approximation. But the uncertainties due to numerical errors can generally be minimized by resolution studies, a careful choice of problem, and a detailed comparison with analytic solutions. This is as true for the hydrodynamic shearing box as for any other problem, although there are not many known analytic solutions that can serve as tests. The shearing-wave solutions presented in this paper constitute one such test problem.

Recently, the two-dimensional form of the shearing wave has been simulated by Johnson & Gammie (2005b) and by Shen et al. (2006). These two studies used two different simulation codes: Johnson & Gammie (2005b) used the operator-split, nonconservative finite-difference ZEUS algorithm (Stone & Norman 1992), and Shen et al. (2006) used the conservative Godunov Athena algorithm (Gardiner & Stone 2005). Here we have carried out a few simple simulations using the Athena code to test the three-dimensional solutions developed in this paper. We have examined the evolution of a single linear shearing wave using the piecewise parabolic (third-order) representation of the underlying variables and the Harten, Lax, van Leer with contact (HLLC) flux option of the Athena code (Gardiner & Stone 2005).

In general, a wave propagated by a finite difference algorithm will be subject to numerical truncation error, which is typically proportional to some power of the ratio of the grid resolution divided by the wavelength. The Athena code has a formal truncation error that is second order, and tests carried out by Shen et al. (2006) with two-dimensional shearing waves showed convergence to the analytic solution at a rate of $N^{-2.5}$ over a range from $N = 64$ to 256 grid zones. An interesting aspect of this test problem is that the radial wavenumber of a shearing wave evolves with time as the wave becomes increasingly tightly wrapped (eq. [26]). Thus, the effective resolution of any localized disturbance declines with time, regardless of the number of grid zones used. Shen et al. (2006) found that once a wave passed to fewer than 16 grid zones per wavelength, its amplitude decayed noticeably and smoothly as the resolution further diminished. Since the dissipation in Athena is strongly nonlinear, a wave will be damped as its wavelength approaches $2\Delta x$, where $\Delta x$ is a fiducial grid interval; Shen et al. observed no aliasing of trailing into leading waves.

The specific problem we have examined is a Keplerian shearing box with $q = -3/2$, $\Omega = 0.001$, constant initial density $\rho = 1$, using both an isothermal equation of state with sound speed $c_s = 4.08\Omega$ and an adiabatic equation of state with $\gamma = 5/3$ and $P = 10^{-6}$. The computational domain has unit lengths, $L_R = L_\phi = L_z = 1$. In local Cartesian coordinates $dx = dR$, $dy = R\,d\phi$, the initial condition for the shearing wave is

$$u_R = A_R \sin\left[2\pi(n_R x + n_\phi y + n_z z)\right], \tag{60}$$

where $n_i$ is the number of wavelengths within the domain at $t = 0$, $n_R = 0$, $n_\phi = 1$, and $n_z = 4$, corresponding to $\beta = 4$. This initial condition is particularly convenient; $u_\phi$ and $u_z$ are zero at $t = 0$. The initial wave amplitude $A_R$ is set to $10^{-5}$ for the adiabatic simulation. We run the problem using $64^3$, $128^3$, and $256^3$ grid zones. Figure 2 shows the evolution of the three velocity components for this mode in the $256^3$ simulation overlaid on the analytic solution (*dashed line*). Some systematic deviation from the analytic solution becomes noticeable beyond $n_R = 16$, which corresponds to 16 grid zones per radial wavelength for the $256^3$ grid-zone resolution. Small-amplitude, high-frequency sound waves can also be seen.

The effect of resolution is illustrated in Figure 3, which plots the wave kinetic energy as a function of time for each of the three grid resolutions along with the analytic value (*dashed line*). As one would expect, as resolution increases the numerical solution maintains close adherence to the analytic value at higher $n_R$ values. Comparison of the fractional error for $n_R < 10$ shows that between $128^3$ and $256^3$ zones the results are converging at the expected second-order rate. The isothermal equation of state simulations

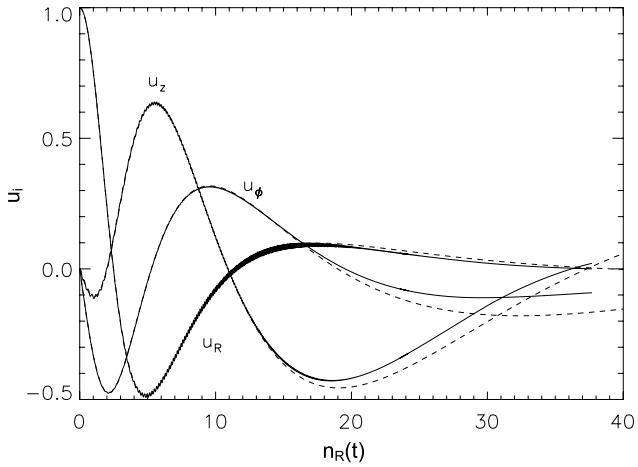



FIG. 2.—Amplitudes for radial ($u_R$), azimuthal ($u_\phi$), and axial ($u_z$) velocity components for a $\beta = 4$ wave, computed in a Keplerian shearing sheet using $256^3$ grid zones. The dashed lines are the exact solutions derived from direct integration of the ODE.

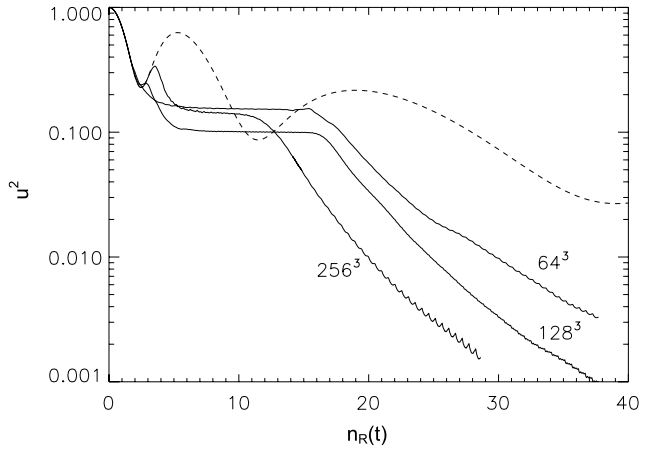



FIG. 4.—Kinetic energy (as a fraction of the input value) in the velocity perturbations for a $\beta = 4$ Keplerian shearing-sheet simulation that began with a large initial amplitude. Shown are lines for $64^3$, $128^3$, and $256^3$ grid zones. The dashed line is the analytic solution for the kinetic energy.

are similar, although they deviate from the analytic value at an earlier time, suggesting that some of the difference is due to compressibility effects in addition to numerical sources of error.

One reason that these shearing waves were of interest in previous two-dimensional studies was that they are amplified during their leading phase. They reach a peak amplitude when $\tau = 0$; beyond that point they are trailing, and their amplitude declines. Numerical simulations offer a way to investigate the effects of compressibility and the stability of the waves as their peak velocity amplitudes approach the level of the background shear or the sound speed. Using $1024^2$ grid-zone two-dimensional simulations, Shen et al. (2006) examined large-amplitude waves and found that, for either leading or trailing waves, the waves become unstable when

$$\left|k_R u_\phi\right| \gtrsim |d\Omega/d\ln R|. \tag{61}$$

When this limit is exceeded, the waves rapidly break down.

As a simple study of large amplitudes in three dimensions we start the $\beta = 4$ shearing-wave mode at $\tau = 0$, as above, but with a large amplitude, namely, $A_R = 0.002$. At this amplitude the stability criterion (61) will be violated when $\delta u_\phi$ reaches its peak at $n_R \sim 2$. This wave was evolved using $64^3$, $128^3$, and $256^3$ grid zones. Figure 4 shows the evolution of the kinetic energy in the velocity perturbations as a function of time. All three resolutions show a breakdown of the wave solution, although with increasing resolution the energy tracks the analytic solution for a slightly longer period of time before breaking down. The wave undergoes what appears to be a Kelvin-Helmholtz instability (Shen et al. 2006). The radial and azimuthal velocity amplitudes drop rapidly, leaving mainly vertical motions that have a finite $n_R$ but are nearly axisymmetric and $z$-independent. This flow subsequently breaks down, again in a manner resembling a Kelvin-Helmholtz instability, and the wave kinetic energy rapidly decays. Interestingly, the higher resolution simulation shows the most rapid decline in perturbed kinetic energy. Thus, while the high-resolution simulations track the analytic solutions longer, they break down faster. This is perhaps a reflection of the fact that the highest resolved wavenumbers have the most rapid Kelvin-Helmholtz growth rates. The lower resolution simulations take longer for the secondary instability to affect the vertical columns. As with the two-dimensional simulations, at late times the perturbed kinetic energy drops toward zero as does the (positive) Reynolds stress. There is no hint of sustained turbulence.

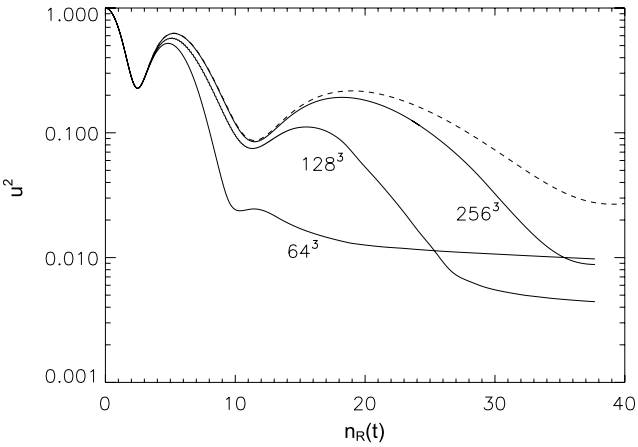



FIG. 3.—Kinetic energy (as a fraction of the input value) in the velocity perturbations for a $\beta = 4$ Keplerian shearing-sheet simulation. The labeled solid lines correspond to simulations using $64^3$, $128^3$, and $256^3$ grid zones. The dashed line is the analytic solution for the kinetic energy.

## 6. DISCUSSION AND CONCLUSION

We have argued that the growing behavior of the $\tau < 0$ phase of local disk perturbations that has been put forth as a possible origin of sustained Keplerian turbulence will not, in fact, lead to such behavior. It is true that an arbitrarily large leading wavenumber will formally produce an arbitrarily large amplification factor during this phase of the evolution. The difficulty is that the linear and nonlinear behavior of the equations is the same for these incompressible plane-wave solutions. The fact that the amplitudes become temporarily large does not change their wave character. Moreover, it appears that in the initial strongly leading configuration, the large shear in the wave is unstable, dissipating the disturbance at small amplitude before it has time to grow.

True disk turbulence requires a tap into a permanent source of free energy, not large wave amplitudes. It is misleading to view the MRI and shear layer turbulence as a consequence of large-amplitude perturbations. These flows are turbulent, because there is a free energy path between the differential rotation and the

perturbations, and it is already present at small amplitudes. The ensuing turbulent cascade is generally not characterized by large-amplitude disturbances.

The outcomes of numerical simulations form a coherent and interrelated pattern of results. For example, Stone & Balbus (1996) studied the behavior of convective turbulence in Keplerian disks as a source of angular momentum transport. The correlation tensor $\langle u_R u_\phi \rangle$, a measure of the angular momentum flux, was found to be tiny. Moreover, it had the wrong sign (radially inward). Although not a direct investigation of Keplerian stability, these results make sense only if the underlying disk is stably stratified, and numerical diffusion is largely absent; reverse angular momentum transport is just what is expected in any Rayleigh-stable nonmagnetized disk that is driven externally (Balbus 2001). Detailed direct studies of Keplerian stability by Balbus et al. (1996) and Hawley et al. (1999) demonstrated nonlinear stability once more, even when the disks were strongly nonlinearly driven. Proponents of transient amplification as a route to turbulence must argue that the very large and tightly wound wavenumbers needed to enter into the nonlinear regime are inaccessible to current codes. But if *this* were the problem, one could simply start the calculation in the nonlinear regime. Flows that are nonlinearly unstable are in fact quite sensitive to starting amplitudes. When this is done for Keplerian disks, no transitions to sustained turbulence are found. Indeed, excellent convergence of all stable flows was found in the study by Hawley et al. (1999), even though the codes involved had completely different dissipative properties.

The fact that the plane-wave solution we have found is exact to all orders in its amplitude suggests that coupling between the disturbance and the background is limited to simple wave-action conservation. This is not a route to turbulence. A superposition of such plane-wave solutions would exhibit group velocity dispersive spreading and nonlinear wave-wave interactions; the latter would impart power to smaller scales. Unless the fluid is itself externally driven, however, there is nothing to sustain the fluctuations against these losses.

Because our solution is inviscid and three-dimensional, it provides an excellent diagnostic for probing the large dynamical range properties of numerical schemes. The solution is strictly exact only for constant density fluids, but the velocity components of an adiabatic fluid are accurately described by our solution. The large-$|\tau|$ behavior and peak amplitudes are stringent tests of a numerical scheme. The disagreement between the analytic and numerical large-$|\tau|$ behavior is particularly revealing, since it shows that the codes are able to uncover more complicated secondary features, even at very small scales. The most obvious effect in this work is compressibility, but the small-scale Kelvin-Helmholtz instability reported by Shen et al. (2006) during the tightly wrapped phase of the wave evolution (when $|u_R| \ll |u_\phi|$) was unforeseen. A strongly leading shearing wave never even reaches the predicted analytic amplitude; its initial intrinsic shear is too unstable. Numerical, analytic, and laboratory studies appear to have reached a robust consensus: without additional flow dynamics, Keplerian rotation is locally nonlinear stable.

This work was supported in part by NASA grants NAG5-13288 and NNG 04-GK77G. S. A. B. also received support from a Chaire d'Excellence award from the Ministry of Higher Education of France. We thank Tom Gardiner and James Stone for valuable discussions on both the Athena code and shearing waves, and the referee for constructive comments. The simulations were carried out on the TeraGrid system at NCSA.

REFERENCES

Afshordi, N., Mukhopadhyay, B., & Narayan, R. 2005, ApJ, 629, 373
Balbus, S. A. 2001, ApJ, 562, 909
———. 2003, ARA&A, 41, 555
Balbus, S. A., & Hawley, J. F. 1998, Rev. Mod. Phys., 70, 1
Balbus, S. A., Hawley, J. F., & Stone, J. M. 1996, ApJ, 467, 76
Bayley, B. J., Orszag, S. A., & Herbert, T. 1988, Ann. Rev. Fluid Mech., 20, 359
Chagelishvili, G. D., Zahn, J.-P., Tevadze, A. G., & Lomidadze, J. G. 2003, A&A, 402, 401
Drazin, P. G., & Reid, W. H. 1981, Hydrodynamic Stability (Cambridge: Cambridge Univ. Press)
Gardiner, T., & Stone, J. M. 2005, J. Comput. Phys., 205, 509
Goldreich, P., Goodman, J., & Narayan, R. 1986, MNRAS, 221, 339
Goldreich, P., & Lynden-Bell, D. 1965, MNRAS, 130, 125
Hawley, J. F., Balbus, S. A., & Winters, W. F. 1999, ApJ, 518, 394
Infeld, E., & Rowlands, G. 1990, Nonlinear Waves, Solitons, and Chaos (Cambridge: Cambridge Univ. Press)
Johnson, B. M., & Gammie, C. F. 2005a, ApJ, 626, 978
———. 2005b, ApJ, 635, 149
Lesur, G., & Longaretti, P.-Y. 2005, A&A, 444, 25
Richard, D. 2001, Ph.D. thesis, Univ. Paris 7
Richard, D., & Zahn, J.-P. 1999, A&A, 347, 734
Shen, Y., Stone, J. M., & Gardiner, T. A. 2006, ApJ, in press (astro-ph/0609131)
Sisan, D. R., Mujica, N., Tillotson, W. A., Huang, Y.-M., Dorland, W., Hassam, A. B., Antonsen, T. M., & Lathrop, D. P. 2004, Phys. Rev. Lett., 93, 114502
Stone, J. M., & Balbus, S. A. 1996, ApJ, 464, 364
Stone, J. M., & Norman, M. L. 1992, ApJS, 80, 753
Zahn, J.-P., Toomre, J., & Spiegel, E. A. 1974, J. Fluid Mech., 64, 319